Identification of room temperature photoluminescence in pseudomorphic modulation-doped AlGaAs/InGaAs/GaAs quantum wells

Wu Lu[a)] and Geok-Ing Ng
School of Electrical and Electronic Engineering, Nanyang Technological University, Singapore 639798, Singapore

B. Jogai
University Research Center, Wright State University, Dayton, Ohio 45435

Jin-Hee Lee and Chul-Soon Park
Semiconductor Division, ETRI, Taejon 305-350, Korea

(Received 20 September 1996; accepted for publication 21 April 1997)

Room temperature photoluminescence in δ-doped pseudomorphic AlGaAs/InGaAs/GaAs quantum wells is investigated. The electron and hole subband structure and optical transition matrix elements are calculated by a self-consistent theoretical method. Separations of the calculated conduction subband levels and valence subband levels reveal that the dominant emissions are due to the transitions from the second electron subband to the first heavy-hole subband, the first electron subband to the first heavy-hole subband, and the first electron subband to the second heavy-hole subband. The calculation also predicts that the transition energies shift to lower energies with the increase of the δ-doping level. This is accounted for by the lowering of the confined levels originating from electrostatically induced band bending. The calculated transition matrix elements demonstrate that transitions with different electron and hole subband indices, i.e., forbidden pairs, are preferred. The relative magnitudes of the squared optical matrix elements for the transitions from the first and second electron subbands to the first heavy-hole subband are analyzed as functions of separations of the first two electron subbands and the first two heavy-hole subbands, respectively. The results show that the 2-1 pair has a larger oscillator strength than the 1-1 and 1-2 pairs in agreement with observations. © *1997 American Institute of Physics.* [S0021-8979(97)01915-4]

I. INTRODUCTION

Modulation-doped quantum wells (MDQWs) are of great interest in the study of two-dimensional electron gas (2DEG) systems, from both scientific and technological viewpoints. These structures provide a nearly ideal system for the study of many-body effects.[1] Pseudomorphic high electron mobility transistors (pHEMTs) with modulation-doped channels have shown excellent performance in low noise, power microwave, and high-speed digital applications.[2–4] Novel optoelectronic devices that employ an electrically controllable charge density in a quantum well (QW) have been proposed.[5]

In AlGaAs/InGaAs/GaAs structures, electrons are confined by two heterojunctions in addition to their electrostatic attraction to ionized impurities in the large gap AlGaAs layer. The InGaAs QW also confines photogenerated holes to the same layer as the electrons. The InGaAs QW greatly enhances the photoluminescence (PL) efficiency due to the strong wave function overlap of electrons and holes and makes PL a valuable tool in investigating the properties of MDQWs and the crystalline quality of the structures.[6] PL has an advantage over other characterization techniques in that it is nondestructive. Additionally, it can yield both low and room temperature spectra, which, in turn, can provide valuable information about the interactions of photoexcited holes with electrons in the 2DEG of such structures.

For a theoretical analysis of the data, classical methods are unsuitable because of the formation of quantized states in the δ and InGaAs layers. More realistic quantum-mechanical methods are needed to properly design device structures and optimize device performances. PL peaks can best be identified by the separations of calculated conduction and valence subband levels. For instance, with the help of such calculations, Ye *et al.*[7] were able to show that the transition from the first electron subband to the second heavy hole subband for single-sided doped pHEMT structures is very sensitive to the separation between the first two heavy hole levels, and for double-sided doped structures, the relative intensities of transitions from the first and second electron subbands to the first heavy hole subband transitions were analyzed as a function of the separation of the Fermi level and the second electron subband level. In this article, through a self-consistent quantum-mechanical calculation for the band structures and transition energies, we analyze the dominant emissions from AlGaAs/InGaAs/GaAs MDQWs at room temperature and investigate the influence of different δ-doping levels on optical transitions between electron and heavy hole subbands in the QW.

II. EXPERIMENT

The samples in our study were grown by molecular beam epitaxy (MBE) in a Riber MBE45 system. A schematic cross section of the structure is shown in Fig. 1. The structure consists of the following layers grown sequentially, from the bottom to the top, on a semi-insulating GaAs sub-

[a)]Electronic mail: eluwu@ntuvax.ntu.ac.sg

Copyright ©2001. All Rights Reserved.

n^+-GaAs 5×10^{18} cm^{-3} 50 Å
i-$Al_{0.3}Ga_{0.7}As$ 400 Å
Si δ-doped plane
i-$Al_{0.3}Ga_{0.7}As$ 30 Å
i-$In_{0.15}Ga_{0.85}As$ 130 Å
i-GaAs 6000Å
S/L GaAs/AlAs
S. I. GaAs substrate

FIG. 1. Cross sectional structure of pHEMT samples A and B. The δ-doping densities of sample A and B are 4.0×10^{12} and $7.0\times10^{12}/\mathrm{cm}^2$, respectively.

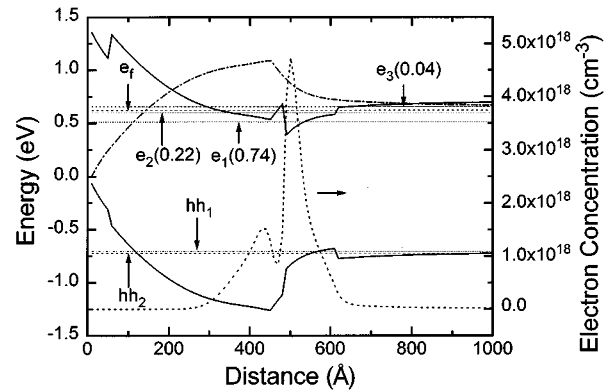

FIG. 2. Self-consistent calculation of the band structure (solid lines), free electron density (dotted line), electrostatic potential (dot-dashed line), Fermi level e_f, excited electron states e_i ($i=1,2,3$), and excited heavy-hole state hh_j ($j=1,2$) which are localized in the $In_{0.15}Ga_{0.85}As$ well for sample A at 300 K. The values in parentheses are the probability densities of the corresponding electron subband levels.

strate: 6000 Å GaAs with 10 superlattices of AlAs/GaAs as a buffer layer, 130 Å undoped InGaAs strained layer, 30 Å AlGaAs spacer, Si δ-doping plane, 400 Å i-AlGaAs source layer, and a Si-doped 50 Å n^+-GaAs cap layer. The two samples, designated as A and B, have the same geometry but different δ-doping densities of 4.0×10^{12} and $7.0\times10^{12}/\mathrm{cm}^2$, respectively. The Al mole fraction in the AlGaAs layers is 0.3 and the In mole fraction in the InGaAs channel layer is 0.15.

For PL measurements, the excitation was provided by a 514.5 nm line form an Ar^+ laser at a typical power density of ~5 W/cm^2. The emission signal from the sample was detected by a cooled InGaAs pin photodiode and a lock-in amplifier. All PL measurements were performed at room temperature with the resolution of 2 Å in wavelength.

III. CALCULATION

The theoretical model we used is similar to that described in Refs. 8 and 9. The four-band $\mathbf{k}\cdot\mathbf{p}$ Hamiltonian and the Poisson equation were solved simultaneously to obtain the band structures. The eigen states were described in terms of a basis set consisting of electron, heavy-hole, light-hole, and split-off bulk states. The exchange-correlation potential was calculated from density functional theory within the local-density approximation. Strain is induced in detail. Both strain-induced band mixing and strain-induced corrections to the spin-orbit interaction are included. The former includes a k-dependent part. Surface donor and acceptor states were included to account for the Fermi-level pinning known to occur near midgap for a free surface of GaAs. Figure 2 shows the calculated conduction and valence band edges and carrier concentration as a function of depth from the surface of sample A at 300 K. To determine in which layer a state is localized, we integrate the probability, defined as the wave function squared, over a certain interval along the growth direction, and assert that the state with the biggest probability is localized in that region. In Fig. 2, the levels of the subbands localized in the channel layer are shown. The probability densities of the electron subbands localized in the channel layer also are given in Fig. 2. These are calculated by the ratio of the electron concentration contained in each subband localized in the channel layer to the total electrons confined in the channel layer. From Fig. 2, we know that the δ-doping plane above the QW causes strong band bending in the spacer layer and in the region near the spacer layer in the QW, and, in part, induces an almost flat-band profile in the region away from the spacer layer. Another contributing factor to the flatness is the requirement that the interior must be electrically resulted. To investigate the observed transition intensities, we calculated the squares of the transition matrix elements, which are proportional to transition rates[10] and are defined as

$$Q_{ij}=\frac{2}{m_0}|\epsilon\cdot\langle\psi_i|\mathbf{P}|\psi_j\rangle|^2, \tag{1}$$

where i and j are the indices of the electron subbands and valence subbands, respectively, ϵ is the unit vector of electric field direction, ψ is electron and hole wave functions, $\mathbf{P}$ is the momentum operator, and m_0 is the free electron mass.

IV. RESULTS AND DISCUSSION

PL results of the two samples are shown in Fig. 3. Clearly, the peaks centered at 1.423 eV are the typical emission of GaAs at room temperature from buffer layers. The peaks from the InGaAs channel layer shift to lower energy along with the increase of δ-doping density. For the PL spectra of AlGaAs/InGaAs/GaAs MDQWs, it is important to determine from which layers the emissions originate and between which electron subbands and hole subbands the transitions occur. To check this feature, we calculated energy separations of conduction and valence subband levels for the structure with various doping densities as shown in Fig. 4. For sample A, two peaks are centered at 1.287 and 1.236 eV, respectively. The first peak at 1.287 eV is identified as a

Copyright ©2001. All Rights Reserved.

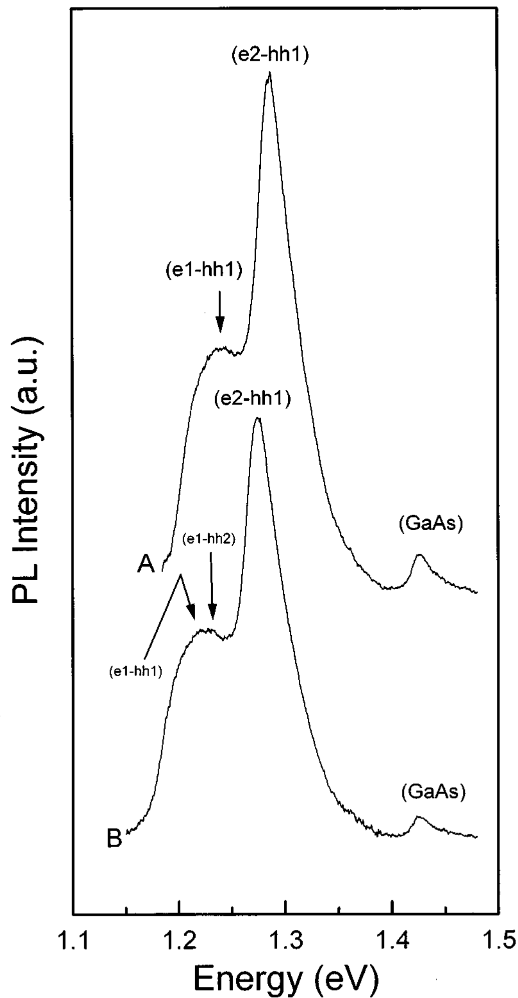

FIG. 3. PL spectra of samples A and B at 300 K.

recombination between the second electron and the first heavy-hole state localized in the InGaAs channel and, accordingly, is designated as $(e_2-\mathrm{hh}_1)$. This transition has a calculated energy separation of 1.282 eV, close to the measured energy. The corresponding squared transition matrix

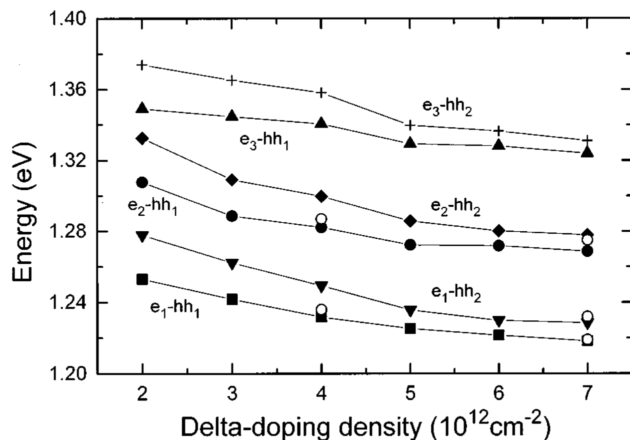

FIG. 4. Calculated transition energies as a function of δ-doping density. Open circles represent the measured values of samples A and B for comparisons.

element Q_{21} is 6.871 eV. The second peak at 1.236 eV is attributed to the transition between the first electron subband and the first heavy-hole subband, $(e_1-\mathrm{hh}_1)$. The corresponding calculated energy separation is 1.232 eV, several meV lower than the measured energy. The squared transition matrix element, Q_{11} is 1.137 eV. Similarly, for sample B, the peak at 1.275 eV is the dominant emission of $(e_2-\mathrm{hh}_1)$. Accordingly, the calculated energy separation of e_2 and hh_1 is 1.269 eV. The square of the transition matrix element is 6.139 eV. But for the lower energy part of the spectrum, a more detailed investigation reveals that it is the overlap of two small peaks at 1.219 and 1.232 eV, respectively. This was deduced through (1) repeated measurements that showed that the two small peaks are indeed emissions and not noise and (2) the corresponding calculated energy separation for $(e_1-\mathrm{hh}_1)$ and $(e-\mathrm{hh}_2)$. These are 1.218 and 1.229 eV, respectively, a little lower than the measured energies. The squares of the transition matrix elements, Q_{11} and Q_{12}, are 0.271 and 0.872 eV, respectively. The transition feature of $(e_1-\mathrm{hh}_2)$ is very sensitive to the degree of hole thermal excitation, which depends on the value of $\mathrm{hh}_1-\mathrm{hh}_2$.[9] Furthermore, although the third electron subband is confined in the QW, it is so close to the top of the well that it becomes unbound for relatively small carrier concentrations, as shown in Fig. 2. For our samples, emissions involving the third electron subband were not detected.

Now we discuss the transition energy changes with δ-doping levels. This is also a very interesting feature of AlGaAs/InGaAs/GaAs QWs. The effect on band bending is obtained by calculating the transition energies in terms of the doping levels in the δ-doping plane. As shown in Fig. 4, the calculated results predict a redshift with the increase of δ-doping density. The calculated magnitudes of the shift for the two peaks, $(e_1-\mathrm{hh}_1)$ and $(e_1-\mathrm{hh}_2)$ are 14 and 12 meV, respectively, which match well with the corresponding shifts of 17 and 12 meV, respectively. These shifts are essentially Stark shifts caused by electrostatically induced band bending. The differences ΔE between the calculated transition energy separations for the doped and undoped QWs can be deduced from the first-order perturbation theory,[11] applicable here because of the proportional relationship between the changes ΔE and the perturbation potential. The correction to the energy of the confined levels can be written as $E_i^{(1)} = \langle \psi_i^{(1)} | \alpha z^2 | \psi_i^{(0)} \rangle$, where α is a constant that is proportional to carrier densities, z is the distance, i represents electrons, heavy holes, or light holes, and indices (1) and (0) represent the two states with and without doping for the triangular and square QWs. This expression always takes on the sign of α. For the structures we investigated, $E_e^{(1)}$ is negative and $E_{\mathrm{hh}}^{(1)}$ is positive. In case of heavy holes, the effective mass is of the order of 10 times that of electrons. As a result, $\psi_e^{(0)}$ and $\psi_{\mathrm{hh}}^{(0)}$ are very different. Therefore, a shift of the change in the transition energy, $\Delta E = E_e^{(1)} + E_{\mathrm{hh}}^{(1)}$, is expected and obtained, as shown in Fig. 4. That ΔE is negative shows that the dominant component of the shift is caused by the shift of the electronic states. Comparing the ΔE of $(e_1-\mathrm{hh}_1)$ with that of $(e_2-\mathrm{hh}_1)$, the shift of $(e_1-\mathrm{hh}_1)$ is larger than that of $(e_2-\mathrm{hh}_1)$ because the ground state is more sensitive to changes in the local electric field induced by changes in the

Copyright ©2001. All Rights Reserved.

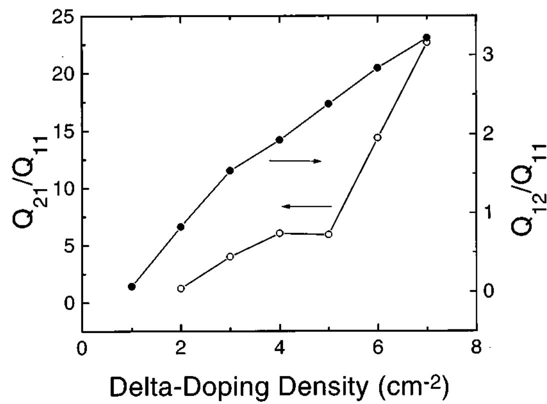

FIG. 5. The ratios of calculated squared transition matrix elements Q_{21}, Q_{12} to Q_{11} at different δ-doping densities.

δ-doping density than by more energetic states.

It is interesting to compare the relative intensities of the different transitions. Clearly, the intensity of $(e_2-\mathrm{hh}_1)$ is much higher than that of $(e_1-\mathrm{hh}_1)$. The experimental results shown in Fig. 3 give us an indication that the intensity of $(e_2-\mathrm{hh}_1)$ is stronger than that of $(e_1-\mathrm{hh}_1)$, and along with the decrement of δ-doping levels, the $(e_1-\mathrm{hh}_2)$ transition will be too small to be observed. To investigate this feature, we calculated the squares of optical transition matrix elements. Figure 5 shows the calculated Q_{21}/Q_{11} and Q_{12}/Q_{11} for the structures we investigated at different δ-doping densities. Along with the increase of δ-doping levels, both Q_{21}/Q_{11} and Q_{12}/Q_{11} increase, an indication that the non-parity transitions with different indices of electron subbands and heavy-hole subbands are preferred. This can be explained by the band bending, which results in a mainly triangular potential for the δ-doping plane above InGaAs QW structures. In case of the $(e_1-\mathrm{hh}_2)$ transition, since only a few heavy holes are contained in the second valence band localized in the channel, for the structure with lower δ-doping densities, the intensity of the $(e_1-\mathrm{hh}_2)$ transition is so small compared to the $(e_1-\mathrm{hh}_1)$ transition that it is not observed. Detailed investigations show that the relative squared transition matrix elements, Q_{21}/Q_{11} and Q_{12}/Q_{11}, are exponential functions of the separations of the first two electron subbands and the first two heavy-hole subbands. In Figs. 6 and 7, the calculated values of the relative squared transition matrix elements are fitted to a growth exponential model. The fitting results give us an indication that the relative intensities Q_{21}/Q_{11} and Q_{12}/Q_{11}, are very sensitive to e_2-e_1 and $\mathrm{hh}_1-\mathrm{hh}_2$ for the structures we investigated. When e_2-e_1 increases with the increase of sheet carrier concentration, the band bending becomes sharper. Then, the overlap of the e_1 and hh_1 wave functions decreases and the overlap of the e_2 and hh_1 wave function increases. The value of $\mathrm{hh}_1-\mathrm{hh}_2$ determines the extent of the hole's thermal excitation. Consequently, the room temperature PL characteristics strongly depend on the value of $\mathrm{hh}_1-\mathrm{hh}_2$, which influences the concentration of photoexcited holes contained in the second heavy-hole subband.

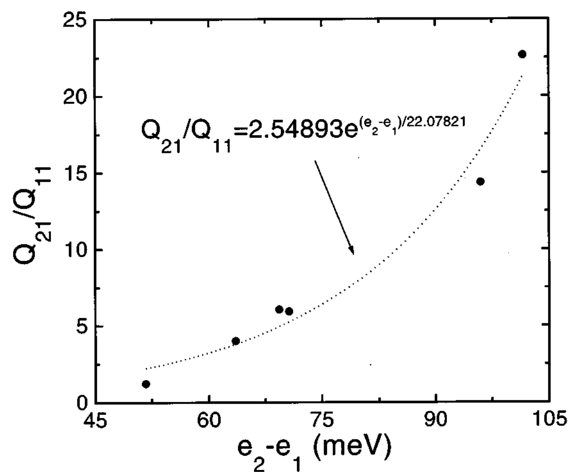

FIG. 6. The ratios of calculated squared transition matrix elements Q_{21} to Q_{11} as a function of the separation of the first two electron subbands. The dashed line is the fit to the exponential growth function. The filled circles represent the calculated values of the relative squared matrix elements.

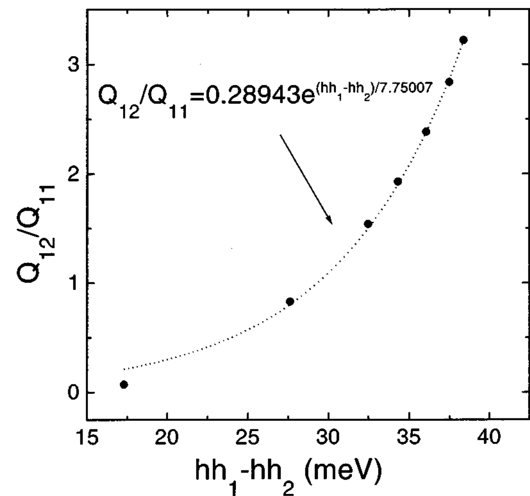

FIG. 7. The ratios of calculated squared transition matrix elements Q_{12} to Q_{11} as a function of the separation of the first two heavy-hole subbands. The dashed line is the fit to the exponential growth function. The filled circles represent the calculated values of the relative squared matrix elements.

V. CONCLUSIONS

A self-consistent band structure calculation demonstrates that the room temperature PL spectra of singly doped pHEMT structures are dominated by $(e_2-\mathrm{hh}_1)$, $(e_1-\mathrm{hh}_1)$, and $(e_1-\mathrm{hh}_2)$ transitions. With a decrease of the δ-doping density, the PL peaks shift to higher energies. The calculated shifts are consistent with the experimental results, and are explained by the change of confined levels due to band bending. The calculated squared optical transition matrix elements show that parity-forbidden transitions are preferred. This result is not surprising, since the QW is shown in the

Copyright ©2001. All Rights Reserved.

present work to be strongly asymmetric. The relative values of the squared transition matrix elements are analyzed in terms of an exponential growth function of separations of the first two electron subbands or the first two heavy-hole subbands.

ACKNOWLEDGMENTS

The authors are indebted to Dr. Hae-Gwon Lee and Dr. Seung-Won Lee for sample growth and PL measurements. One of the authors (W. L.) acknowledges the support of the postdoctoral fellowship program of National Science and Technology Board of Singapore. The work of one author (B. J.) was supported under USAF Contract No. F33615-95-C-1619.

[1] S. Schmitt-Rink, C. Ell, and H. Haug, Phys. Rev. B **33**, 1183 (1986).
[2] J. H. Lee, H. S. Yoon, C. S. Park, and H. M. Park, IEEE Electron Device Lett. **EDL-16**, 271 (1995).
[3] P. Smith, P. Chao, J. Ballingall, and A. Swansen, Microw. J. **33**, 71 (1990).
[4] M. Abe and T. Mimura, IEEE J. Solid-State Circuits **26**, 1337 (1991).
[5] A. Kastalsky, J. H. Abeles, and R. F. Lejeny, Appl. Phys. Lett. **50**, 708 (1987).
[6] A. Dodabalapur, V. P. Kesan, D. R. Hinson, D. P. Neikirk, and B. G. Streetman, Appl. Phys. Lett. **54**, 1675 (1989).
[7] P. W. Yu, B. Jogai, T. J. Rogers, P. A. Martin, and J. M. Ballingall, J. Appl. Phys. **76**, 7535 (1994).
[8] B. Jogai, J. Appl. Phys. **76**, 2316 (1994).
[9] B. Jogai, P. W. Yu, and D. C. Streit, J. Appl. Phys. **75**, 1586 (1994).
[10] See, for example, K. Seeger, *Semiconductor Physics* (Springer, New York, 1991), Chap. 11.
[11] G. Livescu, D. Miller, D. S. Chemla, M. Ramaswamy, T. Y. Chang, N. Sauer, A. C. Gossard, and J. H. English, IEEE J. Quantum Electron. **24**, 1677 (1988).

Copyright ©2001. All Rights Reserved.

Journal of Applied Physics is copyrighted by AIP Publishing LLC (AIP). Reuse of AIP content is subject to the terms at: http://scitation.aip.org/termsconditions. For more information, see http://publishing.aip.org/authors/rights-and-permissions.